

# Spin relaxation in $n$ -type GaAs quantum wells with transient spin grating

M. Q. Weng\* and M. W. Wu†

*Hefei National Laboratory for Physical Sciences at Microscale,  
University of Science and Technology of China, Hefei, Anhui, 230026, China and  
Department of Physics, University of Science and Technology of China, Hefei, Anhui, 230026, China†*

H. L. Cui

*Department of Physics and Engineering Physics,  
Stevens Institute of Technology, Hoboken, NJ 07030, USA*

(Dated: February 8, 2022)

By solving the kinetic spin Bloch equations, we study the time evolution of the transient spin grating, whose spin polarization varies periodically in real space, confined in (001) GaAs quantum wells. With this study we can investigate the properties of both the spin transport and the spin relaxation at the same time. The Fourier component of the spin signal decays double exponentially with two decay rates  $1/\tau_+$  and  $1/\tau_-$ . In high temperature regime, the average of these two rates varies with the grating wave-vector  $q$  quadratically, i.e.,  $(1/\tau_+ + 1/\tau_-)/2 = D_s q^2 + 1/\tilde{\tau}_s$ , with  $D_s$  and  $\tilde{\tau}_s$  representing the spin diffusion coefficient and the average of the out-of-plane and the in-plane spin relaxation times respectively.  $\tau_{\pm}$  calculated from our theory are in good agreement with the experimental data by Weber *et al.* [Phys. Rev. Lett. **98**, 076604 (2007)]. By comparing  $D_s$  with and without the electron-electron Coulomb scattering, we calculate the contribution of Coulomb drag to the spin diffusion coefficient. With the transient spin grating result, we further reveal the relations among different characteristic parameters such as spin diffusion coefficient  $D_s$ , spin relaxation time  $\tau_s$ , and spin injection length  $L_s$ . We show that in the presence of the Dresselhaus and/or Rashba spin-orbit coupling, the widely used relation  $L_s = \sqrt{D_s \tau_s}$  is generally inaccurate and can even be very wrong in some special cases. We present an accurate way to extract the steady-state transport characteristic parameters from the transient spin grating signals.

PACS numbers: 72.25.-b, 72.25.Rb, 72.25.Dc, 75.40.Gb, 71.10.-w

## I. INTRODUCTION

Recently a lot of efforts have been devoted to the study of spin dynamics and spin transport in semiconductor nano-structures in order to realize the spintronic device.<sup>1,2,3,4</sup> In  $n$ -type zinc-blende semiconductors, electron spins are randomized by the Dresselhaus and/or the Rashba spin-orbit coupling (SOC) which acts as an effective magnetic field  $\mathbf{h}(\mathbf{k})$  with its direction and magnitude depending on the electron momentum  $\mathbf{k}$ .<sup>5,6,7</sup> In spatial homogeneous system the spin evolution is characterized by the spin relaxation time  $\tau_s$  which describes the decay rate of spin polarization; The steady-state spin transport is characterized mainly by the spin injection/diffusion length  $L_s$ ,<sup>8,9,10,11</sup> while the transient spin propagation is characterized by spin diffusion coefficient  $D_s$ .<sup>12,13</sup> The relations among these three parameters and other parameters such as momentum relaxation time  $\tau_p$ , charge diffusion coefficient  $D_c$  and mobility  $\mu$  have been actively discussed.

It is understood that spin relaxation/dephasing is induced by the inhomogeneous broadening due to the SOC together with the (spin conserving) scattering.<sup>14,15</sup> The scattering provides a channel to speed up the spin dephasing but also slows down the spin dephasing by weakening the inhomogeneous broadening.<sup>16</sup> The competing effects of scattering have different results on spin dephasing in different conditions. In weak SOC or strong scattering regime, the out-of-plane spin relaxation time

is expected to be  $1/\tau_s \propto \langle \mathbf{h}^2(\mathbf{k}) \tau_p^* \rangle$ . It should be noted that  $\tau_p^*$  not only includes the contribution from conventional momentum scattering mechanisms such as electron-impurity and electron-phonon scattering, but also includes the contribution from electron-electron Coulomb scattering which does not directly affect the charge transport properties.<sup>14,16,17</sup> As for the steady-state spin injection problem, by assuming that the spin dynamics can be separated into two independent processes, spin diffusion and spin relaxation, the spin polarization is expected to decay exponentially along the injection direction with decay “rate”, i.e., the spin injection length,  $L_s = \sqrt{D_s \tau_s}$ , where  $D_s$  and  $\tau_s$  are two phenomenal parameters whose relations with other properties are yet to be determined.<sup>8,9,10,11</sup> However in the presence of the SOC, it has been proved that this assumption is oversimplified. By solving the kinetic spin Bloch equations, it is shown that the effective magnetic field due to the SOC alone causes the electron spin to precess in real space even in diffusive regime.<sup>18,19</sup> The spin polarization varies in the space as  $e^{-x/L_s} \cos(x/L_0)$  instead of simple exponential decay. The spin injection length  $L_s$  and the spatial oscillation “period”  $L_0$  are obtained by solving the kinetic spin Bloch equations,<sup>20</sup> the spin transport equations which include the contribution of the SOC<sup>21</sup> or the linear response theory.<sup>22</sup> In the diffusive regime,  $L_s$  and  $L_0$  can be expressed by SOC strength and momentum scattering time.<sup>20,21,22</sup> As for the spin diffusion coefficient, it was widely assumed to be the same as

the charge diffusion coefficient. Later it was pointed out that spin Coulomb drag (SCD), caused by the electron-electron Coulomb scattering, should suppress the relative motion of electrons with different spins and thus reduce  $D_s$ .<sup>13,23,24,25</sup>

A direct measurement of spin diffusion coefficient can be carried out by transient spin grating (TSG) experiments.<sup>12,13,26,27</sup> With the assumption that spin diffusion and spin relaxation are independent of each other, the decay rate of TSG was written as  $\Gamma_q = D_s q^2 + 1/\tau_s$ , where  $q$  is the wave-vector of the spin grating.<sup>12,13</sup> However, from the lesson of steady-state spin injection one learns that the spin diffusion and relaxation are not separable even in the diffusive regime. This is further justified by the fact that the decay of TSG can be fitted to a double-exponential form instead of single exponential one.<sup>27</sup> It is therefore still a question of how to get spin diffusion coefficient through TSG experiments.

In this article we study the temporal evolution of the TSG by solving the kinetic spin Bloch equations. This paper is organized as following: In Sec. II we first set up the kinetic spin Bloch equations and apply them to solve

the TSG problem. Then we show the analytical solution of simplified equations and the numerical results of the full kinetic spin Bloch equations. In Sec. III we study the relations among the spin relaxation time  $\tau_s$  of a spatially homogeneous system, the spin injection length  $L_s$  and the spatial oscillation period  $L_0$  of the steady-state spin transport as well as  $D_s$  of the transient spin transport. We conclude in Sec. IV.

## II. KINETIC SPIN BLOCH EQUATIONS

The system we study is the electron gas confined in a (001) GaAs quantum well (QW) with width  $a$  grown along the  $z$ -axis. We assume that the well width is narrow enough so that only the lowest subband is occupied. With the help of the nonequilibrium Green function method,<sup>28</sup> one can write down the kinetic spin Bloch equations<sup>4,18,19</sup> by using gradient expansion and generalized Kadanoff-Baym ansatz:

$$\begin{aligned} & \frac{\partial \rho_{\mathbf{k}}(x, t)}{\partial t} + eE(x) \frac{\partial \rho_{\mathbf{k}}(x, t)}{\partial k_x} - \frac{k_x}{m} \frac{\partial \rho_{\mathbf{k}}(x, t)}{\partial x} - i[(g\mu_B \mathbf{B} + \mathbf{h}(\mathbf{k})) \cdot \boldsymbol{\sigma}/2 + \varepsilon_{\text{HF}}(x, \mathbf{k}, t), \rho_{\mathbf{k}}(x, t)] \\ & = \left. \frac{\partial \rho_{\mathbf{k}}(x, t)}{\partial t} \right|_{\text{s}}. \end{aligned} \quad (1)$$

Here we assume that the transport direction is along the  $x$ -axis.  $\rho(x, \mathbf{k}, t)$  is the density matrix whose diagonal elements  $f_{\mathbf{k}\sigma}(x, t)$  represent the electron distribution functions with spin  $\sigma (= \pm 1/2)$  and momentum  $\mathbf{k} = (k_x, k_y)$  at position  $x$ . The off-diagonal elements stand for the spin correlations between spin-up and -down electrons. The second and third terms of Eq. (1) correspond to the drift driven by the electric field  $E(x)$ , determined

by the Poisson equation, and the diffusion of electrons, respectively. The fourth term describes the spin precession around the total magnetic field which is composed of the external magnetic field  $\mathbf{B}$ , the effective magnetic field  $\mathbf{h}(\mathbf{k})$  due to the SOC as well as the one from the Hartree-Fock term of the electron-electron Coulomb interaction  $\varepsilon_{\text{HF}}(x, \mathbf{k}, t)$ .  $\mathbf{h}(\mathbf{k})$  contains the Dresselhaus and the Rashba terms:<sup>5,6,7</sup>

$$\begin{aligned} \mathbf{h}(\mathbf{k}) = & \beta(-k_x \cos 2\theta + k_y \sin 2\theta, k_x \sin 2\theta + k_y \cos 2\theta, 0) \\ & + \gamma \left( \frac{k_x^2 - k_y^2}{2} \sin 2\theta + k_x k_y \cos 2\theta \right) (k_y, -k_x, 0) + \alpha(k_y, -k_x, 0), \end{aligned} \quad (2)$$

where  $\theta$  is the angle between  $x$ -axis (the spin injection/diffusion direction) and the (100) crystal axis.<sup>29</sup>  $\beta = \gamma\pi^2/a^2$  with  $\gamma$  being the Dresselhaus coefficient.<sup>5,6</sup>  $\alpha$  represents the Rashba parameter which depends on the electric field along the growth direction of the QW. The scattering term  $\left. \frac{\partial \rho_{\mathbf{k}}(x, t)}{\partial t} \right|_{\text{s}}$  includes all the scattering, i.e.,

the electron-impurity, the electron-phonon and most importantly the electron-electron Coulomb scattering. It is noted that in our calculation the electron-electron interaction is treated beyond the Hartree-Fock approximation. The expressions for the Hartree-Fock and the scattering terms are given in detail in Ref. 30.

The kinetic spin Bloch equations describe the spin dynamics in the presence of drift, diffusion and spin precession. By choosing some specified initial and boundary conditions, one can obtain the evolution of the spin signal in time and real space by solving these equations for different systems. In order to study the TSG, the initial spin polarization of the electrons is chosen to be a sinusoidal wave along the  $x$ -direction  $P(x) = (N_\uparrow(x) - N_\downarrow(x))/(N_\uparrow(x) + N_\downarrow(x)) = P_0 \sin(x/L)$  but uniform along the  $y$ -axis, where  $L = 2\pi/q$  is the spatial period. Using periodical boundary condition, one only needs to study the dynamics in one period of the space regime.

Unless one makes some simplifications, the kinetic spin Bloch equations are too complicated to be solved analytically. In this paper, we first present an analytical solution

in the diffusive regime using simplified equations. This solution can only provide an intuitive vision of the TSG dynamics. We then present the numerical solution of the full kinetic spin Bloch equations.

### A. Simplified Solution

By neglecting the Hartree-Fock term, the inelastic scattering such as the electron-phonon and the electron-electron Coulomb scatterings and the coupling to the Poisson equation, one is able to rewrite Eq. (1) in diffusive regime when the scattering is strong enough, by using a similar method for calculating the spin relaxation as in Refs. 5,6,

$$\begin{aligned} & \frac{\partial \bar{\mathbf{S}}(q, t)}{\partial t} + Dq^2 \bar{\mathbf{S}}(q, t) + iq\bar{\mathbf{h}} \times \bar{\mathbf{S}}(q, t) \\ & + \frac{1}{2} \begin{pmatrix} (\alpha^2 + \hat{\beta}^2 - 2\alpha\hat{\beta} \sin 2\theta) \langle k^2 \tau_1 \rangle + \langle (\gamma k^3)^2 \tau_3 \rangle / 16 & 2\alpha\hat{\beta} \langle k^2 \tau_1 \rangle \cos 2\theta & 0 \\ 2\alpha\hat{\beta} \langle k^2 \tau_1 \rangle \cos 2\theta & (\alpha^2 + \hat{\beta}^2 + 2\alpha\hat{\beta} \sin 2\theta) \langle k^2 \tau_1 \rangle + \langle (\gamma k^3)^2 \tau_3 \rangle / 16 & 0 \\ 0 & 0 & 2(\alpha^2 + \hat{\beta}^2) \langle k^2 \tau_1 \rangle + \langle (\gamma k^3)^2 \tau_3 \rangle / 8 \end{pmatrix} \bar{\mathbf{S}}(q, t) = 0. \end{aligned} \quad (3)$$

Here  $\bar{\mathbf{S}}(q, t) = \int d^2\mathbf{k} \text{Tr}\{\rho(q, \mathbf{k}, t) \boldsymbol{\sigma}\} d\theta$  is the Fourier component of the spin density function. The second term represents the diffusion term with the diffusion constant  $D = \langle k^2 \tau_1 / 2m^2 \rangle$ .  $1/\tau_l = \int_0^{2\pi} \frac{1}{\tau(k, \theta)} \cos(l\theta) d\theta / 2\pi$  with  $\tau(k, \theta)$  being the momentum relaxation time due to the electron-impurity scattering. The third term is the spin rotation caused by the non-vanishing net effective magnetic field

$$\bar{\mathbf{h}} = \langle k^2 \tau_1 / m \rangle (-\hat{\beta} \cos 2\theta, \hat{\beta} \sin 2\theta - \alpha, 0) \quad (4)$$

due to the DP effect and the diffusion. The last term is the spin relaxation caused by the DP effect and the spin conserving scattering. For a system not far away from the equilibrium,  $\langle \dots \rangle = \int \dots \partial f(\varepsilon_{\mathbf{k}}) / \partial \varepsilon_{\mathbf{k}} d^2\mathbf{k} / \int \partial f(\varepsilon_{\mathbf{k}}) / \partial \varepsilon_{\mathbf{k}} d^2\mathbf{k}$  with  $f(\varepsilon)$  being the Fermi distribution function. It is noted that similar results at low temperature have been obtained by different approach recently.<sup>21</sup>

In the presence of both the Dresselhaus and the Rashba terms, the spin relaxation rates are highly anisotropic. In the weak SOC regime, the in-plane spin relaxation rates are characterized by two decay rates  $\langle (\alpha \pm \hat{\beta})^2 k^2 \tau_1 \rangle / 2 + \gamma^2 \langle k^6 \tau_3 \rangle / 32$ , corresponding to the spin relaxation along the characterized directions (110) and (1 $\bar{1}$ 0) axes respectively. While the out-of-plane relaxation rate is the sum of these two rates  $1/\tau_s = \langle (\alpha^2 + \hat{\beta}^2) k^2 \tau_1 \rangle + \gamma^2 \langle k^6 \tau_3 \rangle / 16$ . Note that, for the quasi-two-dimension system, the presence of the cubic Dresselhaus term mod-

ifies the coefficient of linear Dresselhaus term  $\beta$  to be  $\hat{\beta} = \beta - \gamma k^2 / 4$ . This relation together with Eq. (3) are briefly derived in the Appendix A. Without the spin rotation term, the evolution of the TSG is characterized by the decay rate  $Dq^2 + 1/\tau_s$ . However, the spin rotation mixes the in-plane and out-of-plane spin dynamics. As a result, the evolution is usually described by three relaxation rates. There are two special cases where the evolution can be described by two relaxation rates. The first one is in the system where only one of the Dresselhaus and Rashba terms is important so that the two in-plane spin dynamics become identical. The other is the spin injection/diffusion along (110) and (1 $\bar{1}$ 0) axes where the net effective magnetic field  $\bar{\mathbf{h}}$  is parallel to one of the characteristic directions of the in-plane spin dynamics. Thus it can only mix the remaining in-plane spin with the out-of-plane spin dynamics. The TSG evolution of these cases has a double-exponential form,

$$S_z(q, t) = S_z(q, 0)(\lambda_+ e^{-t/\tau_+} + \lambda_- e^{-t/\tau_-}) , \quad (5)$$

with relaxation rates

$$\Gamma_{\pm} = \frac{1}{\tau_{\pm}} = Dq^2 + \frac{1}{2} \left( \frac{1}{\tau_{s1}} + \frac{1}{\tau_s} \right) \pm \frac{1}{2\tau_{s2}} \sqrt{1 + \frac{16Dq^2\tau_{s2}^2}{\tau_{s1}'}} , \quad (6)$$

in which

$$\lambda_{\pm} = \frac{1}{2} \left( 1 \pm \frac{1}{\sqrt{1 + 16Dq^2\tau_{s2}^2/\tau_{s1}'}} \right) . \quad (7)$$

Here  $\tau_{s1}$  ( $\tau_{s2}$ ) is the spin relaxation time of the in-plane spin which mixes (does not mix) with the out-plane spin due to the net effective magnetic field. For spin injection/diffusion along (110) axis,  $\tau_{s1} = \langle (\alpha - \hat{\beta})^2 k^2 \tau_1 \rangle / 2 + \gamma^2 \langle k^6 \tau_3 \rangle / 32$  and  $\tau'_{s1} = \langle (\alpha - \hat{\beta})^2 k^2 \tau_1 \rangle / 2$ . For spin injection/diffusion along (1 $\bar{1}$ 0) axis,  $\tau_{s1} = \langle (\alpha + \hat{\beta})^2 k^2 \tau_1 \rangle / 2 + \gamma^2 \langle k^6 \tau_3 \rangle / 32$  and  $\tau'_{s1} = \langle (\alpha + \hat{\beta})^2 k^2 \tau_1 \rangle / 2$ . In the long wave length limit ( $q \ll 1$ ),  $\Gamma_+ \simeq 1/\tau_s + (1 + 4\tau_{s2}/\tau'_{s1})Dq^2$  and  $\Gamma_- \simeq 1/\tau_{s1} + (1 - 4\tau_{s2}/\tau'_{s1})Dq^2$  become quadratic functions of  $q$ , roughly correspond to the out-of-plane and the in-plane relaxation rates respectively. In general both of these two decay rates [Eq. (6)] are no longer simple quadratic functions of  $q$ . If one uses the quadratic fitting to yield the spin diffusion coefficient, one either gets larger (for  $\Gamma_+$ ) or smaller (for  $\Gamma_-$ ) values than the true spin diffusion coefficient. The accurate way to get the information of spin diffusion coefficient should be from the average of these two rates

$$\Gamma = (\Gamma_+ + \Gamma_-)/2 = Dq^2 + (1/\tau_s + 1/\tau_{s1})/2, \quad (8)$$

which differs from the current widely used formula by replacing the spin decay rate by the average of the out-of-plane and in-plane ones.

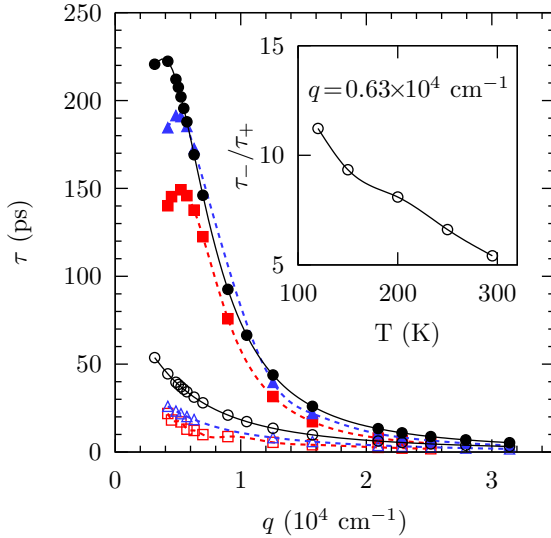


FIG. 1: (Color online) Spin relaxation times  $\tau_+$  (open) and  $\tau_-$  (filled) vs. spin grating wave vector  $q$  for three different temperatures  $T = 120$  (red boxes),  $150$  (blue triangles) and  $295$  K (black circles). The inset is the ratio  $\tau_-/\tau_+$  as a function of temperature for  $q = 0.63 \times 10^4 \text{ cm}^{-1}$ .

## B. Numerical Results

The spin diffusion coefficient obtained by the simplified kinetic spin Bloch equations does not include the contribution of the spin Coulomb drag since the electron-electron Coulomb scattering is neglected. Moreover, the

simplified equations are derived with only the elastic scattering. In the equations all of the relaxation times  $\tau_1$  that appear in the diffusion coefficient  $D$ , net effective magnetic field  $\bar{\mathbf{h}}$  as well as the spin relaxation matrix are the same. For the inelastic electron-phonon scattering, it is still possible to write down Eq. (3) with same relaxation time  $\tau_1$  by the elastic scattering approximation. This approximation is valid only for the electron-acoustic phonon scattering at high temperature and is not valid for the electron-LO phonon scattering. When the Coulomb scattering is important, it gives different contributions to these relaxation times. On the one hand, the relaxation time  $\tau_1$  in the spin relaxation matrix is affected by the whole Coulomb scattering. On the other hand, since the Coulomb scattering among the same spin specie does not change the motion of the center of mass, it does not directly affect the spin diffusion coefficient. Therefore the relaxation time  $\tau_1$  in the spin diffusion coefficient is only affected by part of the Coulomb scattering. For  $\tau_1$  in the net effective magnetic field, it is even more complicated to analyze the role of the Coulomb scattering since it is the joint result of diffusion and spin precession. Therefore the relaxation times  $\tau_1$  in the three different terms should be different in the present of the Coulomb scattering. It would be extremely difficult to get the analytical results when the Coulomb scattering is taken into account. In order to study the drag effect, we numerically solve the full kinetic spin Bloch equations Eq. (1), with all the scattering explicitly included. The numerical scheme is laid out in detail in Appendix B. For simplicity, we first consider the spin diffusion along (100) axis in a symmetrical QW in which the Rashba term vanishes. In our calculation, the SOC strength, the electron and impurity densities, and the QW width are chosen to be  $\gamma = 11.4 \text{ eV}\text{\AA}^3$ ,<sup>31</sup>  $N = 7.8 \times 10^{11} \text{ cm}^{-2}$ ,  $N_i = 1 \times 10^{11} \text{ cm}^{-2}$  and  $a = 12 \text{ nm}$  respectively. The material parameters are listed in detail in Refs. 30.

Our numerical results show that the temporal evolution of TSG can not be fitted by a simple exponential function with desirable accuracy. However, if we use double-exponential function, the accuracy can be improved more than one order of magnitude. This justifies that the temporal evolution of the TSG has indeed double-exponential form in high temperature regime. In Fig. 1 we present the relaxation times of TSG as a function of the grating wave-vector  $q$  for temperatures  $T = 120, 150$  and  $295$  K. It is seen that  $\tau_+$  decreases monotonically as  $q$  increases while  $\tau_-$  has a peak at some small  $q_0$ . The wave-vector of the peak red-shifts when the temperature increases. In the inset of Fig. 1, we show the ratio  $\tau_-/\tau_+$  as the function of temperature for fixed  $q$ . One finds that the ratio decreases with temperature. Our results are in contrast to the predictions of earlier theoretical works that the ratio of these two decay rates and the position of the peak depend only on the SOC and material parameters, but do not vary with the temperature.<sup>22,32</sup> Recent experiment showed that the ratio of these two decay rates are indeed decreases with

the increase of the temperature.<sup>27</sup> It is understood that the temperature dependence of the peak position and ratio between two decay times originate from the cubic  $k$ -term in the Dresselhaus effective magnetic field. In earlier works, it was assumed that only the linear term is important. However, in wide quantum wells with high electron density, the cubic term becomes important. Once the cubic term is considered, the peak  $q_0$  moves from  $q_0 = \sqrt{15}m\beta/2$  (which is independent of temperature) to about  $q_0 = \sqrt{15}m\hat{\beta}/2 = \sqrt{15}m(\beta - \gamma k^2/4)/2$ . Since  $\langle k^2 \rangle$  increases with temperature, thus  $q_0$  decreases. The temperature dependence of  $\tau_+/\tau_-$  also originates from the contribution of the cubic Dresselhaus term.

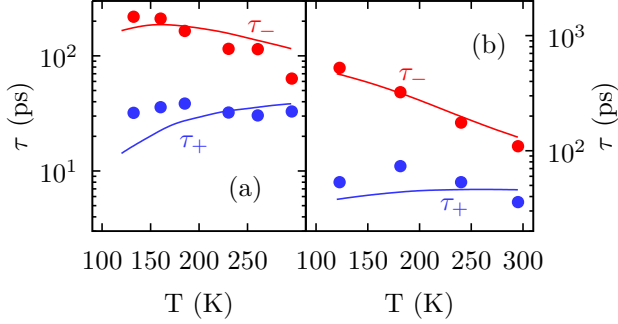


FIG. 2: (Color online) Spin relaxation times  $\tau_{\pm}$  vs. temperature for (a) high-mobility sample with  $q = 0.58 \times 10^4 \text{ cm}^{-1}$  and (b) low-mobility sample with  $q = 0.69 \times 10^4 \text{ cm}^{-1}$ . The dots are the experiment data from Ref. 27.

Due to the natural of the numerical calculation, it is not possible to show the results with all possible parameter combinations. However our qualitative conclusions are valid not just for this particular parameter set but for a large range of parameters. In order to check the quantitative accuracy of our numerical calculation we further show the spin relaxation times as functions of temperature together with the experimental data from Ref. 27 in Fig. 2. Curves in Fig. 2(a) are the theoretical spin relaxation times of high mobility ( $\mu = 1.5 \times 10^4 \text{ cm}^2/\text{Vs}$ ) sample with  $q = 0.58 \times 10^4 \text{ cm}^{-1}$ , while the dots are the experimental data from Ref. 27. Figure 2(b) shows the result of low mobility sample ( $\mu = 3.5 \times 10^3 \text{ cm}^2/\text{Vs}$ ) with  $q = 0.69 \times 10^4 \text{ cm}^{-1}$ . In the calculation we use the finite square well assumption.<sup>31</sup> All the parameters we use are chosen to be the experimental value if available, *eg.* the grating wave-vector, the electron density, the quantum well width, and the impurity concentration determined from the mobility. The only adjustable parameters are the spin-orbit coupling coefficients  $\gamma$  and  $\alpha$ . In the calculation,  $\gamma$  is chosen to be  $11.4 \text{ eV}\text{\AA}^3$  and  $13.8 \text{ eV}\text{\AA}^3$  for the high and low mobility samples respectively and  $\alpha$  is set to be  $0.3\beta$ , close to the choice in Ref. 27. One can see from the figure that our theoretical results are in fairly good agreement with the experiment data.

In Fig. 3, we plot the decay rates  $\Gamma_{\pm} = 1/\tau_{\pm}$  and their average  $\Gamma = (\Gamma_+ + \Gamma_-)/2$  and difference  $\Delta\Gamma = (\Gamma_+ - \Gamma_-)/2$  as functions of  $q$  at  $T = 295 \text{ K}$ . The de-

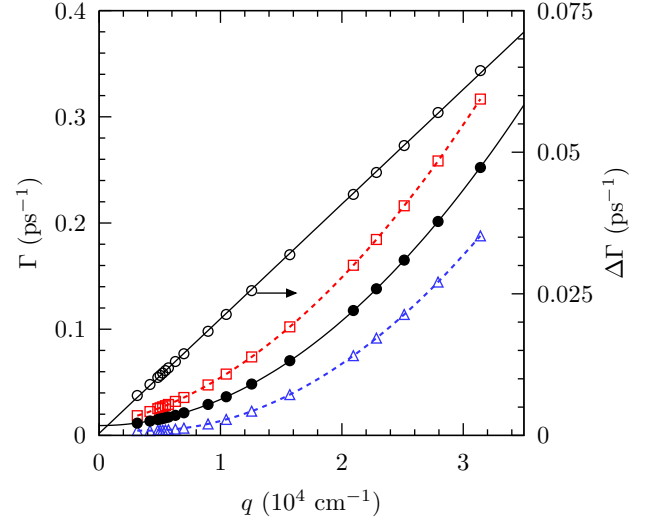


FIG. 3: (Color online)  $\Gamma = (\Gamma_+ + \Gamma_-)/2$  and  $\Delta\Gamma = (\Gamma_+ - \Gamma_-)/2$  vs.  $q$  at  $T = 295 \text{ K}$ . Open boxes/triangles are the relaxation rates  $\Gamma_{+/-}$  calculated from the full kinetic spin Bloch equations. Filled/open circles represent  $\Gamma$  and  $\Delta\Gamma$  respectively. Noted that the scale for  $\Delta\Gamma$  is on the right hand side of the frame. The solid curves are the fitting to  $\Gamma$  and  $\Delta\Gamma$  respectively. The dashed curves are guide to eyes.

cay rates  $\Gamma_{\pm}$  fit poorly with a quadratic function of  $q$ . In contrast, the average decay rate  $\Gamma$  fits pretty well by the function  $\Gamma = D_s q^2 + 1/\tau'_s$ . The resident error of the quadratic fitting for  $\Gamma$  is two orders of magnitude smaller than those of  $\Gamma_{\pm}$ . Moreover we find that  $\tau'_s$  is very close to  $4\tau_s/3$ , inverse of the average of the in-plane and out-of-plane spin relaxation rate. For example, at  $T = 295 \text{ K}$ ,  $\tau'_s$  is about  $107.8 \text{ ps}$  compares to  $4\tau_s/3 = 111.6 \text{ ps}$  with  $\tau_s$  calculated by solving the kinetic spin Bloch equations for spatial uniform system with the same parameters.<sup>16</sup> Inspired by Eq. (8), the coefficient of the quadratic term  $D_s$  can be reasonably assumed to be the spin diffusion coefficient. In this way one can calculate the spin diffusion coefficient with the effect of Coulomb drag included. The difference of  $\Gamma_+$  and  $\Gamma_-$  fits well as a linear function of  $q$ . The linear coefficient of  $\Delta\Gamma$  is about  $2\sqrt{D_s/\tau'_s}$  from Eq. (6).

In Fig. 4 we present the spin diffusion coefficient calculated in the above mentioned method as a function of temperature. For comparison, we also include the charge diffusion coefficient, which is calculated by solving the kinetic spin Bloch equations with the initial condition being the charge gradient instead of the spin gradient. It is clearly seen from the figure that  $D_s < D_c$ . For spin-unpolarized charge diffusion, the electrons move along the same direction and the Coulomb scattering does not change the center-of-mass motion, therefore it does not change the charge diffusion coefficient directly. However, in the spin-polarized transport, spin-up and -down electrons move against each other and the Coulomb scattering therefore slows down the relative motion of these two spin species and reduces spin diffusion coefficient. This

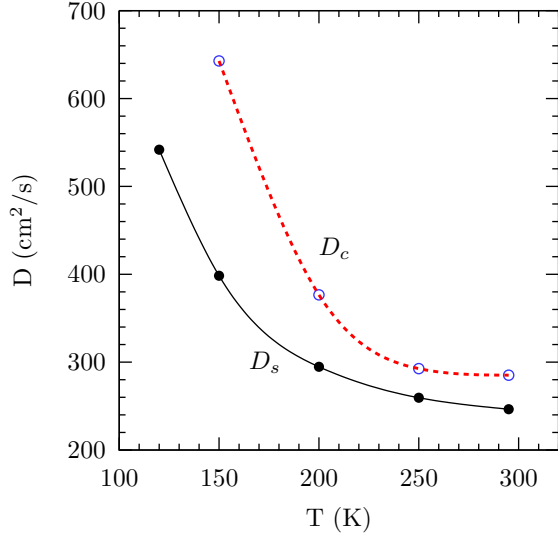


FIG. 4: (Color online) Diffusion coefficient as a function of temperature. Solid circles: Spin diffusion constant  $D_s$  with Coulomb drag; Open circles: Charge diffusion constant  $D_c$ .

is the so-called spin Coulomb drag effect.<sup>23,24,25</sup> From the figure one can tell that, in the temperature regime we study, as the temperature increases, both spin and charge diffusion coefficients decrease and their difference also decreases. Therefore the Coulomb drag is stronger in the low temperature regime. However, even at room temperature the Coulomb drag is still strong enough to reduce the diffusion coefficient by 30 %. These results quantitatively agree with those of Refs. 23,24.

It is also pointed out that the reduction of spin diffusion coefficient mostly comes from the Coulomb drag. The SOC only has slightly effect on the diffusion coefficient since the SOC is very small compared to the Fermi energy. The numerical result shows that removing the SOC only changes spin diffusion coefficient up to one tenth percent for the system we studied.

### III. STEADY-STATE SPIN INJECTION

In this section we discuss how to obtain the steady-state spin injection information from the TSG signal, i.e., to find out the relation between the steady-state spin injection length  $L_s$  and spatial spin oscillation “period”  $L_0$  and the spin diffusion constant  $D_s$  together with the spin relaxation time  $\tau_s$ .

We first show from the simplified solution presented in Sec. II A that the steady-state spin injection can be extracted from the TSG signal by integrating the TSG signal Eq. (5) over the time from 0 to  $\infty$  and the wave-vector from  $-\infty$  to  $\infty$ . Form Eqs. (6) and (7), the integrated TSG reads  $S_z(x) = S_z(0)e^{-x/L_s} \cos(x/L_0 + \psi)$

with

$$L_s = \sqrt[4]{D_s^2 \tau_{s1} \tau_s} / \sin \frac{\phi}{2}, \quad (9)$$

$$L_0 = \sqrt[4]{D_s^2 \tau_{s1} \tau_s} / \cos \frac{\phi}{2}. \quad (10)$$

In these equations

$$\cos \phi = \sqrt{\tau_{s1} \tau_s} (4/\tau'_{s1} - 1/\tau_{s1} - 1/\tau_s)/2. \quad (11)$$

It is noted that if one only considers the Rashba term or the linear Dresselhaus term,  $\tau'_{s1} = \tau_{s1}$ , one then recovers the result  $L_s = 2\sqrt{D_s \tau_s}$  from linear response theory.<sup>22</sup> It is seen that the spin precession actually prolongs the out-of-plane spin injection length by mixing the fast decay of the out-of-plane spin with the slow decay of the in-plane spin. It is further noted from Eq. (9) that *the spin injection length  $L_s$  is generally larger than  $\sqrt{D_s \tau_s}$* . The only exception is when the spin injection is along (110)-direction for the QW with equal linear Dresselhaus and Rashba spin-orbit couplings. In this case  $\theta = \pi/4$ , therefore the net effective magnetic field [Eq. (4)] vanishes. Consequently the in-plane and out-of-plane spin modes do not mix.

For most of the cases,  $L_s$  is in the same order of  $\sqrt{D_s \tau_s}$ , although the former is usually larger. However, there are some special cases where  $\phi \rightarrow 0$ ,  $L_s$  can be *orders of magnitude* different from  $\sqrt{D_s \tau_s}$ . Specifically, according to Cheng *et al.*,<sup>29</sup> when the spin injection/transport direction is along (110) in (001) QW,  $L_s$  becomes larger and larger as  $\alpha$  approaches  $\beta$ , *regardless* of the direction of spin polarization. At the limit of  $\alpha = \beta$ , the spin injection length trends to infinity when the cubic Dresselhaus term is ignored and the spin oscillates with a spatial period of  $2\pi/(2m\beta)$ .<sup>29</sup> As  $\tau_s$  is finite and  $D_s$  changes little for different grating directions, there is no way to obtain infinite  $L_s$  from  $\sqrt{D_s \tau_s}$ .

The infinite injection length and the finite oscillation period can also be understood from the TSG point of view. Without the cubic Dresselhaus term,  $1/\tau_{s2} = (\alpha - \beta)^2 \langle k^2 \tau_1 \rangle / 2$  approaches zero and  $1/\tau_{s1} \rightarrow 1/\tau_s = 2\beta^2 \langle k^2 \tau_1 \rangle$  when  $\alpha \rightarrow \beta$ . Consequently  $\tau_{\pm} = (\sqrt{D}q \pm 1/\sqrt{\tau_s})^{-2}$  when  $\alpha = \beta$ . It is then straightforward to see that  $\tau_-$  becomes infinite provided  $q = q_0 = 1/\sqrt{D\tau_s} = 2m\beta$ . Therefore the steady-state spin injection along (110) axis is dominated by this non-decay TSG mode which is responsible for the infinite spin injection length and the spatial oscillation period  $2\pi/q_0 = 2\pi/(2m\beta)$ .

When the electron-phonon and the electron-electron Coulomb scatterings are taken into account,  $\phi$  should be revised accordingly. Unfortunately, there are no analytical expressions for  $\tau_s$ ,  $\tau_{s1}$  and  $\tau'_{s1}$  when all the scatterings are included. Nevertheless, one can directly use the TSG result to calculate the static injection parameters. The numerical result indicates that the two decay rates obey

$$\Gamma_{\pm} = D_s q^2 + 1/\tau'_s \pm (cq + d) \quad (12)$$

where  $c$  and  $d$  are the fitting parameters to

$$\Delta\Gamma = cq + d. \quad (13)$$

$\alpha$	Injection direction	$D_s$ (cm <sup>2</sup> /s)	$\tau'_s$ (ps)	$c$ ( $\mu\text{m}/\text{ps}$ )	$d$ (ps <sup>-1</sup> )	$L_s^T$ ( $\mu\text{m}$ )	$L_0^T$ ( $\mu\text{m}$ )	$L_s^S$ ( $\mu\text{m}$ )	$L_0^S$ ( $\mu\text{m}$ )
$\alpha = 0$	(100)	246	107.8	0.02	$3.5 \times 10^{-4}$	2.27	2.44	2.28	2.46
$\alpha = \beta$	(110)	243	49.7	$9.4 \times 10^{-3}$	0.012	0.92	5.1	1	4.9
$\alpha = \beta$	(1 $\bar{1}$ 0)	250	28.1	0.058	$-2.7 \times 10^{-3}$	2.7	0.86	2.1	0.9

TABLE I: Comparison of spin injection length  $L_s$  and spatial oscillation length  $L_0$  along different injection directions at  $T = 295$  K from different approaches. The superscripts “S” and “T” stand for  $L_s$  and  $L_0$  obtained from the injection calculation in the steady state and those from TSG parameters by using Eqs. (14) and (15) respectively.

Again by integrating the TSG signal over the time and wave-vector  $q$  with above fitted  $\Gamma_{\pm}$ , one obtains

$$L_s = 2D_s / \sqrt{|c^2 - 4D_s(1/\tau'_s - d)|}, \quad (14)$$

$$L_0 = 2D_s / c. \quad (15)$$

We stress that these two equations give the right spin injection length and the spin oscillation period in the presence of the SOC. From the experiment point of view, one can monitor the time evolution of TSG with different wave-vectors  $q$  and obtain the corresponding decay rates  $\Gamma_{\pm}$ . From the  $q$ -dependence of the decay rates, one can calculate the spin injection length and spin oscillation period from Eqs. (14) and (15). It is noted that Eq. (14) naturally gives the infinite injection length in the special case<sup>29</sup> discussed above as  $c = 2\sqrt{D_s/\tau'_s}$  and  $d = 0$  so that the denominator in Eq. (14) tends to zero. In contrast,  $\sqrt{D_s\tau'_s}$  always remains finite.

In order to check that the accuracy of this approach [Eqs. (14) and (15)], we compare  $L_s$  and  $L_0$  obtained from directly numerically solving the kinetic spin Bloch equations [Eq. (1)] for spin injection in the steady state as described in Refs. 20,29, with those from the TSG approach. In Table I we list  $L_s$  and  $L_0$  obtained from the TSG signal and from the steady-state solution of the kinetic spin Bloch equations for spin injection direction along (100) axis in symmetrical (001) QW, as well as (110) and (1 $\bar{1}$ 0) axes in asymmetrical (001) QW with equal Dresselhaus and Rashba coupling. For the sake of clarity, we also list the corresponding fitted parameters  $\tau'_s$ ,  $c$  and  $d$  in the table. It is noted that in the calculation the cubic Dresselhaus term is included. One can see from the table that even though the injection and the oscillation lengths at different conditions are quite different, the spin diffusion coefficients  $D_s$  are almost the same. Their differences are within the numerical fitting error. This confirms that the SOC is too small compared to the Fermi energy to affect  $D_s$ . Moreover, for all the cases we study,  $L_0$  and  $L_s$  obtained from these two methods agree with each other very well. Although we should point out that the accuracy of  $L_0$  is higher than  $L_s$  due to the numerical error analysis. Since  $c^2 - 4D_s(1/\tau'_s - d)$  is close to 0, its numerical error is much larger than  $c$ . Therefore  $L_s$  calculated from TSG is not as accurate as  $L_0$ .

#### IV. CONCLUSION

In conclusion, we study the evolution of TSG by solving the kinetic spin Bloch equations with periodic boundary condition. From the simplified equations, we analytically show that due to the spin precession the spin signal decays double-exponentially instead of simple exponentially, even in the diffusive regime. *Neither* of these two decay rates are simple quadratic functions of the grating wave-vector  $q$ . However their average value depends quadratically on  $q$  and the corresponding coefficient of the quadratic term is the right diffusion coefficient  $D_s$ . Therefore it is more accurate to yield the diffusion coefficient from  $q$  dependence of the average of the two decay rates.

We further show that the corresponding solution from the full kinetic spin Bloch equations which include all of the scattering mechanisms, especially the Coulomb scattering, is also in the form of the double exponential decay. From the  $q$ -dependence of the average decay rate, one can calculate the spin diffusion coefficient with the Coulomb drag effect included. It is shown that the Coulomb drag effect is stronger in low temperature and decreases with the increase of temperature. However, even at room temperature the Coulomb drag is still an important factor which reduces the spin diffusion coefficient markedly compared to the charge diffusion coefficient.

We also show that by using the TSG result one can obtain the characteristic steady-state transport parameters, such as the injection length and the spatial oscillation length, from diffusion coefficient  $D_s$  and the spin relaxation times. We point out that in a system with the SOC, the widely adopted relation  $L_s = \sqrt{D_s\tau'_s}$  in the literature is generally quantitatively inaccurate and can be even qualitatively wrong for some special cases. The accurate way to extract the spin injection and spatial oscillation lengths directly from the TSG decay rates at different grating wave-vector, which are experimentally measurable, is proposed. We believe this investigation is important in fully understanding the TSG signals in experiment.

#### Acknowledgments

This work was supported by the Natural Science Foundation of China under Grant Nos. 10574120 and



10725417, the National Basic Research Program of China under Grant No. 2006CB922005, the Knowledge Innovation Project of Chinese Academy of Sciences and the US Army Research Office. The authors would like to thank T. Korn for his critical reading of this manuscript. One of the authors (MWW) would like to thank J. Fabian and C. Schüller at Universität Regensburg, Germany for hospitality where this work was finalized, and the Robert-Bosch Stiftung and GRK 638 for financial support.

## APPENDIX A: DERIVATION OF SIMPLIFIED SOLUTION

By using a similar method for calculating the spin relaxation due to the Dresselhaus effect, Eqs. (3) and

$$\begin{aligned} & \frac{\partial \rho_l(q, k, t)}{\partial t} - \frac{ikq}{2m} \left( \rho_{l+1}(q, k, t) + \rho_{l-1}(q, k, t) \right) - i \sum_m \left[ \mathbf{h}_{l-m}(k) \cdot \boldsymbol{\sigma}, \rho_m(q, k, t) \right] \\ & = -\frac{\rho_l(q, k, t)}{\tau_l} (1 - \delta_{l,0}), \end{aligned} \quad (\text{A1})$$

where  $\rho_l(q, k, t) = \int e^{-il\phi} \rho_{\mathbf{k}}(q, t) d\phi / 2\pi$  and  $\mathbf{k} = (k \cos \phi, k \sin \phi, 0)$ . When both the Dresselhaus and the Rashba terms are taken into account,

$$\begin{aligned} \mathbf{h}(\mathbf{k}) &= \gamma k ((\pi/a)^2 - k^2/4) (-\cos \phi, \sin \phi, 0) + \gamma k^3/4 (-\cos 3\phi, -\sin 3\phi, 0) \\ &\quad + \alpha k (\sin \phi, -\cos \phi, 0), \end{aligned} \quad (\text{A2})$$

$$= \hat{\beta} k (-\cos \phi, \sin \phi, 0) + \alpha k (\sin \phi, -\cos \phi, 0) + \gamma k^3/4 (-\cos 3\phi, -\sin 3\phi, 0). \quad (\text{A3})$$

Therefore there are four effective magnetic field components which do not vanish, namely  $\mathbf{h}_{\pm 1}(k)$  and  $\mathbf{h}_{\pm 3}(k)$ . It should be noted that, in quasi-two-dimensional system, the  $\pm 1$  components of the Dresselhaus term are modified by the cubic term  $\hat{\beta} = \gamma[(\pi/a)^2 - k^2/4] = \beta - \gamma k^2/4$ . When the scattering is strong, one can drop the terms with  $\tau_l$  higher than the first order and rearrange Eq. (A1) to obtain Eq. (3). The only difference is that in the spatial inhomogeneous system, we have additional terms relying on the wave-vector  $q$ . These additional terms give rise to the second and third terms in Eq. (3).

## APPENDIX B: NUMERICAL SCHEME

In order to solve the kinetic spin Bloch equations numerically, one has to discretize the real space, the momentum space as well as the time. The real space is divided into segments with equal length. The momentum space is divided into grids of equal energy and angular differences.<sup>30</sup> The second order up-wind differential scheme is applied for the diffusion term and the drift

(4) can be derived by expanding Eq. (1) in angular momentums.<sup>5,6</sup> Neglecting the Hartree-Fock term, the inelastic scattering and the electric field, the Fourier component of the  $l$ -th order of density matrix obeys the following equation:

term. The former reads

$$\frac{k_x}{m} \frac{\partial f(x)}{\partial x} \rightarrow \begin{cases} \frac{k_x}{m} \frac{3f(x) - 4f(x - \Delta x) + f(x - 2\Delta x)}{2\Delta x} & \frac{k_x}{m} > 0 \\ -\frac{k_x}{m} \frac{3f(x) - 4f(x + \Delta x) + f(x + 2\Delta x)}{2\Delta x} & \frac{k_x}{m} < 0 \end{cases}. \quad (\text{B1})$$

The boundary condition for  $x$  is chosen to be the periodic one when we calculate the TSG problem or fixed when we calculate the steady-state injection problem.<sup>20</sup> In the energy ( $\mathcal{E}$ ) and angular ( $\phi$ ) space, the drift term reads

$$\begin{aligned} eE(x) \frac{\partial g(k_x, k_y)}{\partial k_x} &= \frac{eE(x)}{\sqrt{2m}} \left( \frac{\partial}{\partial \mathcal{E}} [2\sqrt{\mathcal{E}} \cos \theta g(\mathcal{E}, \theta)] \right. \\ &\quad \left. - \frac{\partial}{\partial \theta} \frac{g(\mathcal{E}, \theta) \sin \theta}{\sqrt{\mathcal{E}}} \right). \end{aligned} \quad (\text{B2})$$

Similar to the diffusion term, one can easily write down the second order up-wind differential schemes for  $\mathcal{E}$  and  $\theta$  respectively. The numerical schemes for the spin precession and the scattering terms are laid out in detail in Refs. 20,30.

We apply the third order semi-implicit Adams-Bashforth scheme for the time differential<sup>33</sup> to achieve higher accuracy in temporal evolution. This scheme also



saves CPU time. The differential scheme is then given by

$$\begin{aligned} \frac{\rho_{\mathbf{k}}(x, t + \Delta t) - \rho_{\mathbf{k}}(x, t)}{\Delta t} = & \frac{5}{4}F[\rho_{\mathbf{k}}(x, t + \Delta t)] \\ & - F[\rho_{\mathbf{k}}(x, t)] + 3/4F[\rho_{\mathbf{k}}(x, t - \Delta t)] + \frac{23}{12}G[\rho_{\mathbf{k}}(x, t)] \\ & - \frac{16}{12}G[\rho_{\mathbf{k}}(x, t - \Delta t)] + \frac{5}{12}G[\rho_{\mathbf{k}}(x, t - 2\Delta t)]. \quad (\text{B3}) \end{aligned}$$

Here  $F[\rho_{\mathbf{k}}(x, t)]$  denotes the drift and diffusion terms (the second and third terms) in Eq. (1) and  $G[\rho_{\mathbf{k}}(x, t)]$  stands for the spin precession and the scattering terms (the fourth and fifth terms) in Eq. (1). The implicit part of the equation is solved by Jacobian-free Newton-Krylov

algorithm.<sup>34</sup>

The accuracy of the numerical scheme used in this paper is higher than the one used in our previous works.<sup>19,20</sup> The main numerical errors come from the drift and diffusion parts since the grid size of real space and momentum space is limited by the computing power. We find that the accuracy of the temporal evolution does not change the result of the final steady-state spin transport too much. It is therefore expected that the present numerical scheme and the previous one give very close results on the steady-state transport properties. However, the present scheme enables us to also study the time sensitive phenomenons such as the TSG to a sufficient accuracy.

- 
- \* Electronic address: weng@ustc.edu.cn.  
† Electronic address: mwwu@ustc.edu.cn.  
‡ Mailing address.
- <sup>1</sup> S. A. Wolf, J. Supercond. **13**, 195 (2000).
  - <sup>2</sup> *Semiconductor Spintronics and Quantum Computation*, edited by D. D. Awschalom, D. Loss, and N. Samarth (Springer, Berlin, 2002); and references therein.
  - <sup>3</sup> I. Žutić, J. Fabian, and S. D. Sarma, Rev. Mod. Phys. **76**, 323 (2004); J. Fabian, A. Matos-Abiaguea, C. Ertlera, P. Stano, and I. Žutić, acta physica slovacica **57**, 565 (2007); and references therein.
  - <sup>4</sup> M. W. Wu, M. Q. Weng, and J. L. Cheng, in *Physics, Chemistry and Application of Nanostructures: Reviews and Short Notes to Nanomeeting 2007*, edited by V. E. Borisenko, V. S. Gurin, and S. V. Gaponenko (World Scientific, Singapore, 2007), pp. 14; and references therein.
  - <sup>5</sup> M. I. D'yakonov and V. I. Perel', Zh. Eksp. Teor. Fiz. **60**, 1954 (1971), [Sov. Phys.-JETP **33**, 1053 (1971)].
  - <sup>6</sup> M. I. D'yakonov and V. I. Perel', Fiz. Tverd. Tela **13**, 3581 (1971) [Sov. Phys. Solid State **13**, 3023 (1972)].
  - <sup>7</sup> Y. A. Bychkov and E. I. Rashba, Pis'ma Zh. Eksp. Teor. Fiz., **39**, 66 (1984) [JETP Lett. **39**, 78 (1984)].
  - <sup>8</sup> G. Schmidt, D. Ferrand, L. W. Molenkamp, A. T. Filip, and B. J. van Wees, Phys. Rev. B **62**, R4790 (2000).
  - <sup>9</sup> M. E. Flatté and J. M. Byers, Phys. Rev. Lett. **84**, 4220 (2000).
  - <sup>10</sup> I. Žutić, J. Fabian, and S. D. Sarma, Phys. Rev. B **64**, 121201 (2001).
  - <sup>11</sup> I. Žutić, J. Fabian, and S. Das Sarma, Phys. Rev. Lett. **88**, 066603 (2002).
  - <sup>12</sup> A. R. Cameron, P. Riblet, and A. Miller, Phys. Rev. Lett. **76**, 4793 (1996).
  - <sup>13</sup> C. P. Weber, N. Gedik, J. E. Moore, J. Orenstein, J. Stephens, and D. D. Awschalom, Nature **437**, 1330 (2005).
  - <sup>14</sup> M. W. Wu and C. Z. Ning, Eur. Phys. J. B. **18**, 373 (2000).
  - <sup>15</sup> M. W. Wu, J. Phys. Soc. Jpn. **70**, 2195 (2001).
  - <sup>16</sup> M. Q. Weng and M. W. Wu, Phys. Rev. B **68**, 075312 (2003).
  - <sup>17</sup> M. M. Glazov and E. L. Ivchenko, Pis'ma. Zh. Eksp. Teor. Fiz. **75**, 476 (2002) [JETP Lett. **75**, 403 (2002)].
  - <sup>18</sup> M. Q. Weng and M. W. Wu, Phys. Rev. B **66**, 235109 (2002).
  - <sup>19</sup> M. Q. Weng and M. W. Wu, J. Appl. Phys. **93**, 410 (2003).
  - <sup>20</sup> J. L. Cheng and M. W. Wu, J. Appl. Phys. **101**, 073702 (2007).
  - <sup>21</sup> T. D. Stanescu and V. Galitski, Phys. Rev. B **75**, 125307 (2007).
  - <sup>22</sup> A. A. Burkov, A. S. Núñez, and A. H. MacDonald, Phys. Rev. B **70**, 155308 (2004).
  - <sup>23</sup> I. D'Amico and G. Vignale, Phys. Rev. B **65**, 085109 (2002).
  - <sup>24</sup> I. D'Amico and G. Vignale, Phys. Rev. B **68**, 045307 (2003).
  - <sup>25</sup> L. Jiang, M. Q. Weng, M. W. Wu, and J. L. Cheng, J. Appl. Phys. **98**, 113702 (2005).
  - <sup>26</sup> S. G. Carter, Z. Chen, and S. T. Cundiff, Phys. Rev. Lett. **97**, 136602 (2006).
  - <sup>27</sup> C. P. Weber, J. Orenstein, B. Andrei Bernevig, S.-C. Zhang, J. Stephens, and D. D. Awschalom, Phys. Rev. Lett. **98**, 076604 (2007).
  - <sup>28</sup> H. Haug and A. P. Jauho, *Quantum Kinetics in Transport and Optics of Semiconductors* (Springer-Verlag, Berlin, 1996).
  - <sup>29</sup> J. L. Cheng, M. W. Wu, and I. C. da Cunha Lima, Phys. Rev. B **75**, 205328 (2007).
  - <sup>30</sup> M. Q. Weng, M. W. Wu, and L. Jiang, Phys. Rev. B **69**, 245320 (2004).
  - <sup>31</sup> J. Zhou, J. L. Cheng, and M. W. Wu, Phys. Rev. B **75**, 045305 (2007).
  - <sup>32</sup> B. A. Bernevig, J. Orenstein, and S.-C. Zhang, Phys. Rev. Lett. **97**, 236601 (2006).
  - <sup>33</sup> S. R. Fulton, Tech. Rep. 2002-01, Department of Mathematics and Computer Science, Clarkson University, Potsdam, NY (2002).
  - <sup>34</sup> P. N. Brown and Y. Saad, SIAM Journal on Scientific and Statistical Computing **11**, 450 (1990).